

Dynamical mean-field theory study of Nagaoka ferromagnetism

Hyowon Park, K. Haule, C. A. Marianetti, and G. Kotliar

*Department of Physics and Astronomy and Center for Condensed Matter Theory, Rutgers University,
Piscataway, New Jersey 08854-8019, USA*

(Received 30 August 2007; published 7 January 2008)

We revisit Nagaoka ferromagnetism in the $U=\infty$ Hubbard model within the dynamical mean-field theory (DMFT) using the recently developed continuous time quantum Monte Carlo method as the impurity solver. The stability of Nagaoka ferromagnetism is studied as a function of the temperature, the doping level, and the next-nearest-neighbor lattice hopping t' . We found that the nature of the phase transition, as well as the stability of the ferromagnetic state, is very sensitive to the t' hopping. Negative $t'=-0.1t$ stabilizes ferromagnetism up to higher doping levels. The paramagnetic state is reached through a first-order phase transition. Alternatively, a second-order phase transition is observed at $t'=0$. Very near half-filling, the coherence temperature T_{coh} of the paramagnetic metal becomes very low and ferromagnetism evolves out of an incoherent metal rather than conventional Fermi liquid. We use the DMFT results to benchmark slave-boson method which might be useful in more complicated geometries.

DOI: [10.1103/PhysRevB.77.035107](https://doi.org/10.1103/PhysRevB.77.035107)

PACS number(s): 71.27.+a

I. INTRODUCTION

The stability of the ferromagnetic phase in the $U=\infty$ Hubbard model is a long standing problem. Nagaoka¹ showed that for a single hole in a bipartite lattice, the ground state is a fully polarized ferromagnet, and the term “Nagaoka ferromagnetism” is commonly used to describe this state. Whether a fully or a partially polarized phase persists to a finite hole density (δ) is controversial and has been the subject of numerous investigations.²

The problem has been addressed with variational wave functions,^{3–7} slave particle methods,^{8,9} quantum Monte Carlo (QMC) methods,¹⁰ and variational QMC methods.¹¹ In all these methods, the ferromagnetism is stable up to a critical value of doping δ_c . It was also demonstrated by these approaches that the size of the ferromagnetic region depends strongly on the lattice through the electronic dispersion. The ferromagnetic state was found to be unstable even for the case of a single hole in the $U=\infty$ square lattice with a small positive next-nearest-neighbor hopping t' .¹² At an intermediate or a large U , a flat band below the Fermi level¹³ or a peak in the density of states below the Fermi level,^{14–17} as realized in the fcc lattice^{18,19} or a Van Hove singularity,²⁰ stabilizes the ferromagnetic state.

The dynamical mean-field theory (DMFT) has also been used to address the Nagaoka problem, however, the number of available impurity solvers in the $U=\infty$ case is very limited. Obermeier *et al.*²¹ carried out the first DMFT study of this problem using the noncrossing approximation as the impurity solver. They found a partially polarized ferromagnetic state below a critical temperature T_c in the infinite dimensional hypercubic lattice. The existence of a ferromagnetic state in this model was later confirmed by a DMFT study which used numerical renormalization group as the impurity solver.²²

In this study, we revisit the problem of Nagaoka ferromagnetism in the $U=\infty$ Hubbard model within DMFT using the recently developed continuous time quantum Monte Carlo (CTQMC) method as the impurity solver.^{23,24} This im-

purity solver allows the numerically exact solution of the DMFT equations at very low temperatures for all values of doping level δ even in the $U=\infty$ model. We find that at large doping, the ferromagnetism emerges from a conventional Fermi liquid, while at small doping, the Curie temperature is very close to the coherence temperature, hence the ferromagnetism emerges from an incoherent state. We pay particular attention to the possibility of phase separation and its dependence on the sign of t'/t . Finally, we benchmark simpler approaches to the problem such as the slave-boson method. Within slave-boson approach, several physical quantities such as the quasiparticle renormalization amplitude or the susceptibility cannot be determined reliably. Nevertheless, we show that the total energy can be computed quite reliably within the simple slave-boson approach due to error cancellation. This is important since the detailed modeling of optical lattices of cold atoms, which provide a clean realization of the Hubbard model, will require incorporating spatial inhomogeneities into the treatments of strong correlations. At present, this can only be done with simpler techniques such as slave-boson methods.

We study the Hamiltonian of the $U=\infty$ Hubbard model given by

$$\hat{H} = - \sum_{ij\sigma} t_{ij} \hat{P}_s \hat{c}_{i\sigma}^\dagger \hat{c}_{j\sigma} \hat{P}_s, \quad (1)$$

where \hat{P}_s is a projection operator which removes states with double-occupied sites. We choose the lattice dispersion of the two-dimensional square lattice with the nearest-neighbor (nn) hopping t and the next-nearest-neighbor (nnn) hopping t' . The units are fixed by choosing $t=\frac{1}{2}$.

II. DYNAMICAL MEAN-FIELD THEORY PLUS CONTINUOUS TIME QUANTUM MONTE CARLO APPROACH

DMFT maps the partition function of the Hubbard model onto the partition function of an effective Anderson impurity

model (AIM) resulting in the following effective action.

$$S_{eff} = S_{atom} + \int_0^\beta d\tau \int_0^\beta d\tau' \sum_\sigma c_\sigma^\dagger(\tau) \Delta_\sigma(\tau - \tau') c_\sigma(\tau'), \quad (2)$$

where S_{atom} represents the action of the isolated impurity and $\Delta_\sigma(\tau - \tau')$ is the hybridization function of the effective AIM. In this $U = \infty$ case, the double-occupied state of the impurity should be excluded when evaluating S_{atom} . $\Delta_\sigma(\tau - \tau')$ is not initially known and it must be determined by the DMFT self-consistency condition given below. The impurity Green function and the impurity self-energy are given by the following equations:

$$G_\sigma(\tau - \tau') = -\langle T c_\sigma(\tau) c_\sigma^\dagger(\tau') \rangle_{S_{eff}}, \quad (3)$$

$$\Sigma_\sigma(i\omega_n) = i\omega_n + \mu - \Delta_\sigma(i\omega_n) - G_\sigma^{-1}(i\omega_n). \quad (4)$$

The DMFT self-consistency condition requires that the local Green's function of the lattice coincides with the Green's function of the auxiliary AIM and identifies the equivalence between the lattice local self-energy and the self-energy of the corresponding AIM, i.e.,

$$\begin{aligned} & \sum_{\mathbf{k}} \frac{1}{i\omega_n + \mu + h\sigma - \epsilon(\mathbf{k}) - \Sigma_\sigma(i\omega_n)} \\ &= \frac{1}{i\omega_n + \mu + h\sigma - \Delta_\sigma(i\omega_n) - \Sigma_\sigma(i\omega_n)}, \end{aligned} \quad (5)$$

where the lattice dispersion of our choice is $\epsilon(\mathbf{k}) = -2t(\cos k_x + \cos k_y) - 4t' \cos k_x \cos k_y$ and h is the external magnetic field. For a given Weiss field $\Delta_\sigma(i\omega_n)$, the effective action S_{eff} is constructed and the AIM is solved for different $G_\sigma(i\omega_n)$ and $\Sigma_\sigma(i\omega_n)$. Using the self-consistency condition [Eq. (5)], the Weiss field $\Delta_\sigma(i\omega_n)$ is computed. This iterative procedure is repeated until the Green's function is converged.

To solve the impurity problem of Eq. (2), the CTQMC impurity solver is used. In this method, the hybridization part of the effective action is treated as a perturbation around the atomic action and all diagrams are summed up by stochastic Metropolis sampling.²⁴ In this $U = \infty$ case, doubly occupied state of the atom is excluded from atomic eigenstates. CTQMC converges well in the low Matsubara frequency region, but it is poorly behaved in the high frequency region. Therefore, one needs the analytic expression for the self-energy in the high frequency limit and it has to be interpolated to the low frequency region. The high frequency expansion for the $U = \infty$ Hubbard model gives

$$\text{Re}[\Sigma_\sigma(\infty)] = m_{1\sigma}/m_{0\sigma}^2 + \mu, \quad (6)$$

$$\text{Im}[\Sigma_\sigma(\infty)] = (1 - 1/m_{0\sigma})\omega, \quad (7)$$

where $m_{0\sigma} = \langle \{c_\sigma, c_\sigma^\dagger\} \rangle = 1 - n_{-\sigma}$ and $m_{1\sigma} = \langle \{[c_\sigma, H], c_\sigma^\dagger\} \rangle = -\mu(1 - n_{-\sigma}) - \text{Tr}[\Delta_{-\sigma} G_{-\sigma}]$. Note the appearance of the kinetic energy $\text{Tr}[\Delta_{-\sigma} G_{-\sigma}]$ in this expansion which is absent for finite U .

Within CTQMC, various spin dependent physical quantities can be calculated such as occupation numbers (n_\uparrow, n_\downarrow)

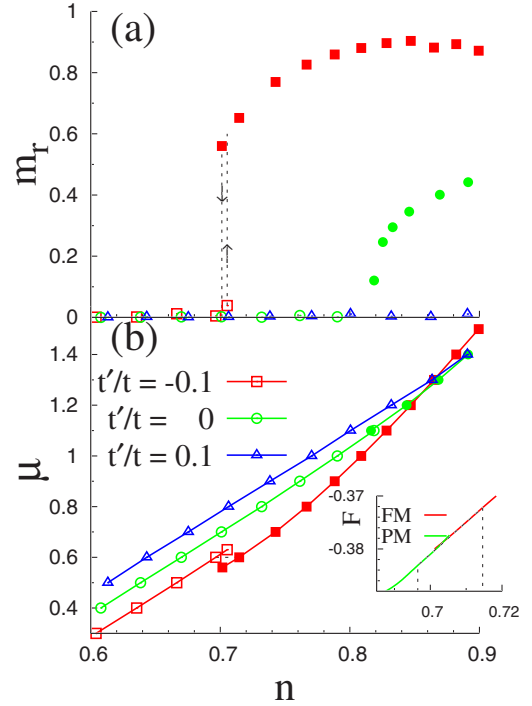


FIG. 1. (Color online) (a) The reduced magnetization $m_r = (n_\uparrow - n_\downarrow)/(n_\uparrow + n_\downarrow)$ vs the electron density n at $t'/t = -0.1, 0$, and 0.1 . (b) The chemical potential μ vs n at $t'/t = -0.1, 0$, and 0.1 . Filled points indicate a FM state. Inset: FM free energy and PM free energy vs n at $t'/t = -0.1$. The dotted line is constructed using the Maxwell construction. All calculations were performed at $T = 0.01$.

and the local magnetic susceptibility (χ_{loc}). The $q=0$ magnetic susceptibility of a lattice can be calculated from χ_{loc} by evaluating the two particle vertex functions, which is a numerically demanding task. To circumvent this difficulty, $\chi_{q=0}$ of a lattice can be calculated from the ratio of magnetization to the external magnetic field ($\chi = \frac{dm}{dh}|_{h=0}$). The external field h alters the effective action [Eq. (2)] by adding $h\sigma$ to atomic energies, and the self-consistency condition [Eq. (5)] is enforced to include the spin dependent $h\sigma$ term during DMFT iterations. The exclusion of the double occupancy ($U = \infty$) implies the Hubbard potential energy to vanish, and the only relevant energy is the kinetic energy. The latter is given by $\text{Tr}[\Delta_\sigma G_\sigma]$, and it is related to the average of the perturbation order k as follows:

$$E_{kin,\sigma} = \text{Tr}[\Delta_\sigma G_\sigma] = -T \langle k_\sigma \rangle, \quad (8)$$

where T is temperature. Therefore, it is possible to calculate the kinetic energy to high accuracy by evaluating $\langle k_\sigma \rangle$. The free energy F can also be derived from the kinetic energy as long as the system is in the Fermi liquid regime,

$$F(T) \cong E_{kin} - \frac{\pi^2}{3} Z^{-1} \rho_0(\mu) T^2, \quad (9)$$

where Z is the renormalization residue and ρ_0 is the noninteracting density of states.

Figure 1(a) shows the reduced magnetization $m_r = (n_\uparrow$

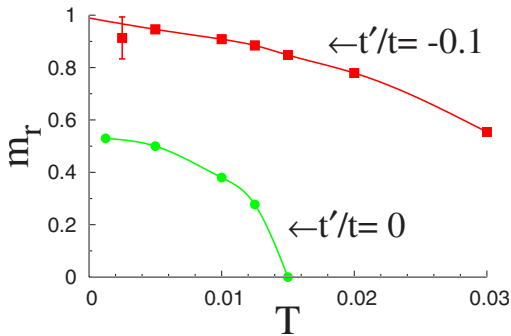


FIG. 2. (Color online) m_r vs T at fixed $n=0.85$ with $t'/t=-0.1$ and 0. The fully polarized FM state ($m_r=1$) is expected only when $t'/t=-0.1$.

$-n_{\downarrow})/(n_{\uparrow}+n_{\downarrow})$ as a function of the electron density n at three distinct t'/t ratios. The result is notably different for different values of t'/t . The spontaneously broken ferromagnetic (FM) state ($m_r \neq 0$) is favored for $t'/t < 0$, while the FM state is unstable for $t'/t > 0$. The critical density (n_c) at which the transition occurs increases as t'/t increases, reducing the region of stability of the FM state. Moreover, at $t'/t=-0.1$, magnetization m_r changes abruptly at $n_c=0.705$ indicating a first-order transition, while at $t'/t=0$, magnetization m_r increases continuously indicating a second-order phase transition at $n_c=0.815$.

Notice that close to half-filling, the Curie temperature is low, and at fixed temperature ($T=0.01$), it becomes increasingly difficult to converge the DMFT equations near the transition temperature due to the standard critical slowing down.

Near half-filling, the quasiparticle bandwidth is small due to strong correlations; hence, the thermal fluctuations are comparable to the Curie temperature in this region. A stable FM state is possible only if T is sufficiently lower than T_{coh} . In the region above 0.95, an incoherent paramagnetic (PM) state becomes stable as T exceeds T_{coh} .

Inspecting the chemical potential as a function of density reveals that the nature of the transition changes with t'/t [see Fig. 1(b)]. For $t'/t=0$, the transition is continuous, while for $t'/t=-0.1$, there is a region of constant chemical potential which corresponds to a first-order transition. The flat chemical potential region ($n=0.696-0.715$) indicates that two different DMFT solutions (FM, PM) can be converged depending on the initial conditions and it indicates phase separation (PS) of the FM and PM states. This region is determined by the Maxwell construction which connects common tangents between two phases in the free energy vs n graph [Fig. 1 (inset)].

The original debate on the Nagaoka problem was focused on the existence of the fully polarized FM state at finite δ in the $T \rightarrow 0$ limit. Therefore, it is necessary to investigate magnetization m_r at very low T . In Fig. 2, we show very low temperature ($T=0.001t$) results, and it is clear that the magnetization saturates to a value smaller than unity for $t'/t=0$ while it reaches unity at low temperatures for $t'/t=-0.1$. The fully polarized Nagaoka state is thus not stable for $t'/t=0$ and moderately small doping ($\delta \sim 0.1$) while it is realized for $t'/t=-0.1$. As the spins become fully polarized ($t'/t=-0.1, T \rightarrow 0$), numerics require high statistics and an error

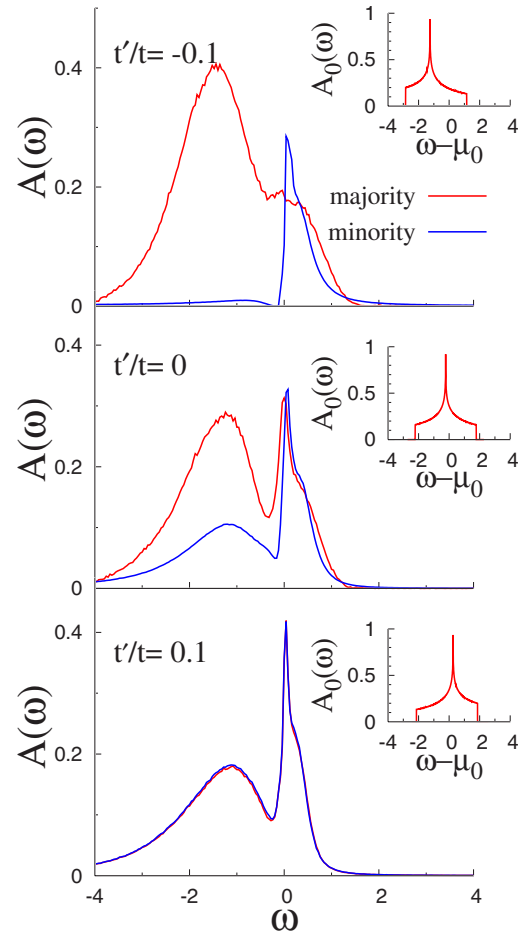


FIG. 3. (Color online) The spectral functions $A(\omega)$ at $t'/t = -0.1$ (top), 0 (middle), and 0.1 (bottom) for fixed $n=0.85$. Inset: noninteracting spectral functions [$A_0(\omega)$] of the majority spin at the corresponding t'/t values. [$\mu_0 = \mu - \text{Re} \Sigma(0)$] All calculations were performed at $T=0.01$.

bar is specified to take into account the numerical error.

The spectral functions are shown in Fig. 3. Since CTQMC delivers response functions on the imaginary frequency axis, one needs to perform the analytical continuation of the Green function to the real axis. Here, we use the maximum entropy method.²⁵ The spectral functions show noticeable differences for small change in t' . At $t'/t=-0.1$, the majority spin spectral function shows a very small renormalization due to interactions ($Z \approx 1$) and a large spectral peak in the occupied part of the spectra. The overall shape is similar to the noninteracting spectral function [Fig. 3 (inset)]. The minority spin spectral function is much more correlated and shows a narrow quasiparticle band above the Fermi level and a tiny lower Hubbard band. In the magnetic state, the occupied part of the spectra is thus well described by a model of a weakly correlated FM metal.

At $t'/t=0$ and $t'/t=0.1$, the spectral functions consist of both the narrow quasiparticle band and the lower Hubbard band. In the $U=\infty$ Hubbard model, the upper Hubbard band disappears due to the exclusion of double occupancy.

The stability of the FM state at $t'/t=-0.1$ can be traced back to the large spectral peak in the occupied part of the

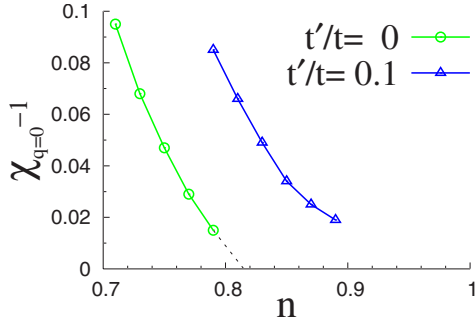


FIG. 4. (Color online) The uniform susceptibility ($\chi_{q=0}^{-1}$) vs n at $t'/t=0$ and 0.1. The dotted line is for the extrapolation to $\chi_{q=0}^{-1}=0$ ($T=0.01$).

spectra of the noninteracting density of states (DOS), as shown in the inset of Fig. 3. As explained above, the majority spin of the FM state shows only weak renormalization due to interactions. This is a consequence of the Pauli exclusion principle which constrains the motion of a hole in the polarized background and interactions, being less important in this case, which do not hamper the coherent motion of the hole through the polarized background. The kinetic energy of this state thus clearly depends on t'/t ratio and is reduced with decreasing t'/t . Contrary to the FM state, the correlations are very strong in the PM state regardless of the spectral peak in the noninteracting DOS and t'/t ratio. The coherent part of the spectra does not contribute much to the kinetic energy as the quasiparticle bandwidth shrinks due to the strong correlations. The incoherent part of the spectra in the form of the Hubbard bands arises from localized electrons and consequently it is almost independent of the specific lattice dispersion. Therefore, the kinetic energy of the PM state weakly depends on t'/t ratio. The peak in the occupied part of the spectra of the noninteracting DOS thus reduces the kinetic energy of the FM state compared to the PM state thus stabilizing ferromagnetism.

It is known from other studies¹³ that a highly degenerate flat band in the occupied part of the spectra favors ferromagnetism at any finite U . However, this flat-band ferromagnetism (an extreme limit of the Stoner ferromagnetism) argument is not applicable to the $t'/t=-0.1$ case of the Nagaoka ferromagnetism (the other extreme limit of the Stoner ferromagnetism). In a flat-band model, the ground state of the noninteracting system is highly degenerate due to the presence of the flat band. However, even a small Coulomb repulsion lowers the energy of the FM state (if the flat band is half-filled) and stabilizes the FM state. The role of the Coulomb interaction is simply to lift the huge degeneracy and “select” the states with the highest magnetization as unique ground states. In the infinite U model, the potential energy vanishes because of no doubly occupancy. However, the kinetic energy depends sensitively on the smoothness of the spin polarized background, and a disordered PM state cannot gain the kinetic energy by the variation of t'/t while a FM state can.

The inverse of the uniform magnetic susceptibility ($\chi_{q=0}^{-1}$) of the PM state vs n at $t'/t=0$ and 0.1 is shown in Fig. 4. The extrapolated line at $t'=0$ indicates that χ diverges near n

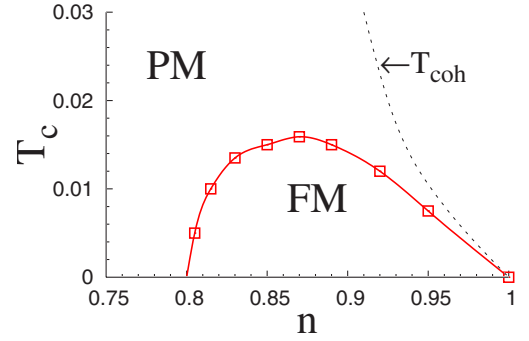


FIG. 5. (Color online) The critical temperature T_c vs n at $t'=0$. n_c at $T=0$ is obtained from the extrapolation. The dotted line represents the coherence temperature T_{coh} vs n .

$=0.815$, confirming the second-order transition at the critical density ($n_c=0.815$). At $t'/t=0.1$, one might expect that χ will diverge near $n=1$. However, as T_{coh} becomes smaller than T near $n=1$, the incoherent PM state is stabilized. In other words, at $t'/t=0.1$, the crossover from the coherent PM state to the incoherent PM state occurs instead of the transition to the FM state.

Figure 5 shows the critical temperature (T_c) vs n at $t'/t=0$. In the region below T_c , a partially polarized FM state is found, and it is determined by observing $n_{\uparrow} \neq n_{\downarrow}$ in a CTQMC result. This graph shows that the lower critical density (n_c) at $T=0$ is around 0.8. At half-filling, critical temperature should vanish due to the following reason. The kinetic energy at half-filling is zero in both the PM and the FM states because of the blocking of charge density. The entropy of the paramagnet is much larger than the entropy of the ferromagnet due to the large spin degeneracy of the PM state. In other words, PM state is thermodynamically stable at any finite temperature at $n=1$.

As the width of the quasiparticle band becomes smaller near $n=1$, the coherence temperature T_{coh} is also reduced, making it hard to sustain the quasiparticle coherent band. At $T > T_{coh}$, the PM state is clearly stabilized. The T_{coh} boundary can be determined from the imaginary part of self-energy [$\text{Im} \Sigma(i\omega_n)$] on the imaginary frequency axis. In a coherent region ($T < T_{coh}$), the renormalization residue Z is well defined ($0 < Z < 1$) by evaluating the negative slope of $\text{Im} \Sigma(i\omega_n)$ at $\omega=0$ [$Z = (1 - \frac{d \text{Im} \Sigma}{d\omega} |_{\omega=0})^{-1}$]. However, in the incoherent regime ($T > T_{coh}$), the slope of $\text{Im} \Sigma(i\omega_n)$ at $\omega=0$ becomes positive, making the concept of Z ill defined (Fig. 7). Therefore, we determined T_{coh} as the temperature where the slope of the low self-energy vanishes, and found that it is almost proportional to $\delta^{3/2}$, in surprising agreement with the findings of a previous study of doped Mott insulator.²⁶

In a two-dimensional Hubbard model, a long-range magnetic order at a finite T is prohibited by the Mermin-Wagner theorem. A FM order is possible only at $T=0$. At any finite T , Goldstone modes disorder the system,²⁷ and it results in a correlation length which is finite but exponentially large in T^{-1} . DMFT does not capture this behavior. Therefore, T_c in the context of the two-dimensional model should be interpreted as an estimate of the temperature where the correla-

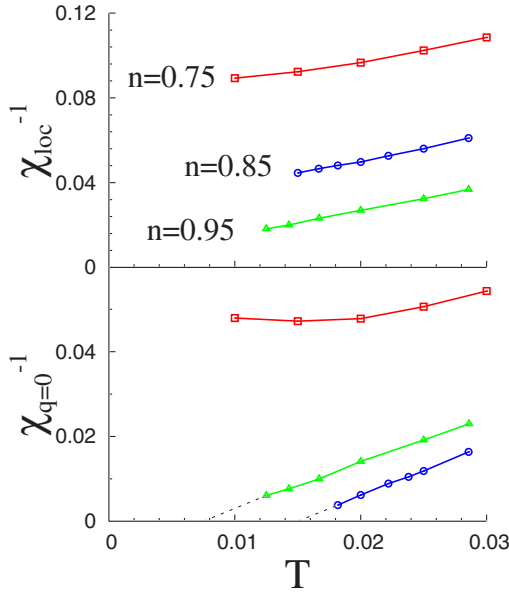


FIG. 6. (Color online) The local susceptibility (χ_{loc}^{-1}) vs T and the uniform susceptibility ($\chi_{q=0}^{-1}$) vs T ($t'/t=0$).

tion length gets very large. In higher dimensions, we expect a FM state at low T with the correct dependence on t'/t . The Nagaoka ferromagnetism study using the dispersion of realistic materials deserves further investigations since the energy balance between a FM state and a PM state or the character of the transition is very sensitive to the details of the lattice structure.

In general, $n_{\uparrow}-n_{\downarrow}$ exhibits small fluctuations near the boundary of T_c due to the finite T . The fluctuations become especially severe through the transition from the FM state to the incoherent PM state near $n=1$. Therefore, the boundary points can be determined more precisely by examining the temperature dependence of $\chi_{q=0}^{-1}$ (Fig. 6). $\chi_{q=0}^{-1}$ near a transition point obeys the Curie-Weiss form ($\chi_{q=0}^{-1} \sim T - T_c$). Both coherent ($n=0.85$) and incoherent ($n=0.95$) regions show linear dependence of $\chi_{q=0}^{-1}$ on T . The $\chi_{q=0}^{-1}$ for $n=0.75$ barely depends on T , exhibiting Pauli paramagnetic behavior. χ_{loc}^{-1} is greater than $\chi_{q=0}^{-1}$ and it increases as n decreases. This is because in DMFT, $\chi_{loc}^{-1} \sim T + T_{coh}$ and T_{coh} increases as n decreases.²⁶

Figure 7 shows the behavior of $\text{Im} \Sigma(i\omega_n)$ for the three different phases in the T_c phase diagram of Fig. 5. For $n=0.85$ and $T=0.01$, a coherent FM state is expected from the phase diagram. A coherent Fermi liquid is validated by investigating the negative slope of $\text{Im} \Sigma(i\omega_n)$ at $\omega=0$. The slope for spin σ at the high frequency part is given by $-n_{-\sigma}/1-n_{-\sigma}$ [Eq. (7)] and the inequality of the slope indicates $n_{\uparrow} \neq n_{\downarrow}$ confirming the FM state. The majority spin state has a smaller slope at high frequency because $n_{-\sigma}$ of the majority spin is smaller than that of the minority spin. Also, because the slope of the majority spin at $\omega=0$ is smaller, Z of the majority spin is larger than that of the minority spin. This means that the quasiparticle band of the minority spin is strongly renormalized by correlations while the majority spin state tends to be similar to the noninteracting energy dispersion. For $n=0.85$ and $T=0.02$, a coherent PM state is estab-

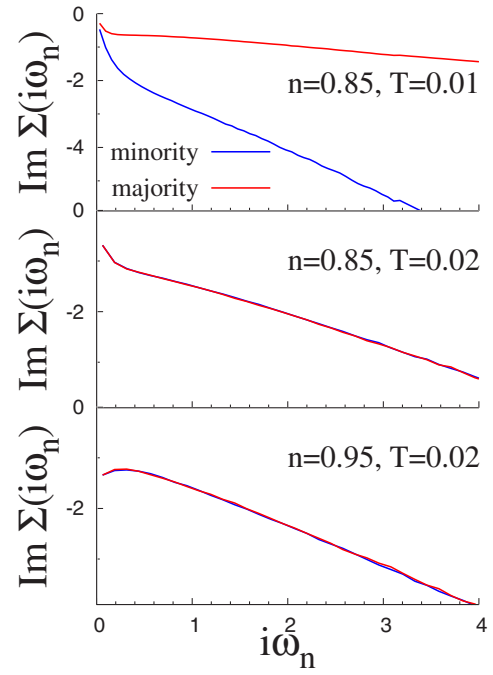


FIG. 7. (Color online) $\text{Im} \Sigma(i\omega_n)$ vs $i\omega_n$ at the coherent FM state (the top panel), the coherent PM state (the middle panel), and the incoherent PM state (the bottom panel) ($t'/t=0$).

lished by observing a negative slope at $\omega=0$ and no spin symmetry breaking. For $n=0.95$ and $T=0.02$, an incoherent PM state is expected from the positive slope at $\omega=0$ because the concept of Z is no longer valid and the application of Fermi liquid theory fails. Lastly, for fixed $T=0.02$, as n increases from 0.85 to 0.95, the slope at high frequency also increases because $n_{-\sigma}$ increases.

III. NAGAOKA FERROMAGNETISM FROM A FOUR-SITE PLAQUETTE

In order to provide a simple interpretation of why decreasing t' stabilizes the Nagaoka state, we examine the simplest possible model which retains the physics of the Nagaoka problem. We consider a four-site plaquette with three electrons (one hole). The ground state of this model may be characterized by the quantum number corresponding to the total spin angular momentum (i.e., $S = \frac{3}{2}, \frac{1}{2}$) and the z direction of the spin angular momentum ($S_z = \pm \frac{3}{2}, S_z = \pm \frac{1}{2}$). The whole Hamiltonian matrix is a 32×32 matrix excluding double-occupied sites, and it is block diagonalized to six distinct spin sectors by performing the unitary transform to the proper S, S_z basis. The ground state energy at each spin sector is determined by the exact diagonalization of Hamiltonian matrix.

The lowest energy in an $S = \frac{3}{2}$ sector is given by $-2t + t'$ and in the $S = \frac{1}{2}$ sector is given by $-\sqrt{3t^2 + t'^2}$, as shown in Fig. 8. The energy dependence of an $S = \frac{3}{2}$ state is noticeably different from that of an $S = \frac{1}{2}$. In an $S = \frac{3}{2}$ case, doubly occupied states are excluded by the Pauli principle regardless of U . Therefore, the $U = \infty$ Hamiltonian is equivalent to the $U = 0$ Hamiltonian where the addition of the positive nnn hop-

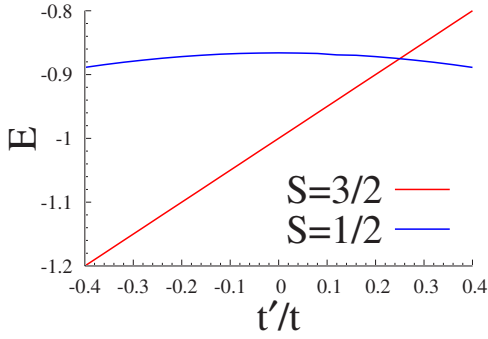


FIG. 8. (Color online) The lowest energies of an $S=1/2$ state and an $S=3/2$ state in a $U=\infty$ four-site toy model varying t'/t . E is the energy in units of $t=1/2$.

ping t' contributes linearly to the increase of the kinetic energy. However, doubly occupied states in an $S=1/2$ sector are excluded only for $U \rightarrow \infty$. Therefore, unlike the $S=3/2$ case, the energy dependence on t' is greatly reduced as the Hilbert space shrinks due to the infinite U .

An $S=3/2$ ground state is indicative of the Nagaoka ferromagnetic state, while an $S=1/2$ ground state is indicative of a paramagnetic state. The $S=3/2$ state is the ground state for $t'/t < 0.24$ and the energy difference increases approximately linearly thereafter indicating that the Nagaoka state is stabilized as t'/t is decreased. This is in qualitative agreement with the DMFT results presented in the previous section. The energy of the $S=1/2$ state weakly depends on t' , while the $S=3/2$ energy decreases as t'/t decreases. This also explains that the stability of Nagaoka ferromagnetism originates from the minimization of the kinetic energy.

IV. MEAN-FIELD SLAVE-BOSON APPROACH

In this section, Nagaoka ferromagnetism in a $U=\infty$ Hubbard model is studied using a mean-field slave-boson approach. In a slave-boson method, a fermion operator is accompanied by bosonic operators (i.e., slave-bosons) which keep track of the local occupation number. The three slave-boson operators are \hat{e} , \hat{p}_\uparrow , and \hat{p}_\downarrow and they act on unoccupied sites, spin-up sites, and spin-down sites, respectively. In this $U=\infty$ case, the doubly occupied sites are excluded. Constraints regarding the conservation of the occupation number are imposed with Lagrange multipliers ($\lambda, \lambda_\uparrow, \lambda_\downarrow$). The slave-boson Hamiltonian is given by

$$\hat{H} = - \sum_{ij\sigma} t_{ij} \hat{c}_{i\sigma}^\dagger \hat{z}_{i\sigma} \hat{c}_{j\sigma} - \sum_{i\sigma} \lambda_{i\sigma} (\hat{p}_{i\sigma}^\dagger \hat{p}_{i\sigma} - \hat{c}_{i\sigma}^\dagger \hat{c}_{i\sigma}) + \sum_{i\sigma} \lambda_i (\hat{p}_{i\sigma}^\dagger \hat{p}_{i\sigma} + \hat{e}_i^\dagger \hat{e}_i - 1), \quad (10)$$

where $\hat{z}_{i\sigma} = \frac{1}{\sqrt{1-\hat{p}_{i\sigma}^\dagger \hat{p}_{i\sigma}}} \hat{e}_i^\dagger \hat{p}_{i\sigma} \frac{1}{\sqrt{1-\hat{e}_i^\dagger \hat{e}_i - \hat{p}_{i\sigma}^\dagger \hat{p}_{i\sigma}}}$. $t_{ij}=t$ if i, j are nn, and $t_{ij}=t'$ if i, j are nnn. The noninteracting $\epsilon(\mathbf{k})$ is taken to be $-2t(\cos k_x + \cos k_y) - 4t' \cos k_x \cos k_y$ as in the previous section. The original Fock space has been enlarged including the slave-boson fields. The partition function can be calculated from the Feynman functional path integral over the original

Fermi fields, slave-boson fields, and Lagrange multipliers. The integral over the Fermi fields is straightforward because the Hamiltonian is quadratic in the Fermi fields. The integral over the slave-boson fields and Lagrange multipliers should be performed using the saddle-point approximation, where the integral over the slave-boson fields and Lagrange multipliers is approximated by setting their space and time independent mean-field values which minimize the Hamiltonian. The physical meaning of slave-boson mean-field value is clear. The expectation value $\langle \hat{e}^\dagger \hat{e} \rangle$ corresponds to the fraction of unoccupied sites, i.e., the hole density $\delta(1-n)$. Similarly, $\langle \hat{p}_\uparrow^\dagger \hat{p}_\uparrow \rangle$ equals to the spin-up occupation number (n_\uparrow), and $\langle \hat{p}_\downarrow^\dagger \hat{p}_\downarrow \rangle$ corresponds to the spin-down occupation number (n_\downarrow).

The free energy can be derived from the partition function ($F = -k_B T \ln Z$) and it is necessary to compare the free energies between ferromagnetic state and paramagnetic state to investigate the transition. The free energy is a function of magnetization $m = n_\uparrow - n_\downarrow$, δ , and T . At $T=0$, the free energy becomes the ground state energy. The energies of the fully polarized ferromagnetic (FPFM) state ($m = n_\uparrow$) and the PM state ($m = 0$) are given by

$$E_{FPFM}(\delta) = \frac{1}{N_s} \sum_{\mathbf{k}} \epsilon(\mathbf{k}) \Theta[\mu - \epsilon(\mathbf{k})], \quad (11)$$

$$E_{PM}(\delta) = \frac{1}{N_s} \sum_{\mathbf{k}, \sigma} Z \epsilon(\mathbf{k}) \Theta[\mu^* - Z \epsilon(\mathbf{k})], \quad (12)$$

where N_s is the number of total sites, Z is the renormalization residue given by $2\delta/(1+\delta)$, μ is the chemical potential in a fully polarized ferromagnetic state satisfying $(1/N_s) \sum_{\mathbf{k}} \Theta[\mu - \epsilon(\mathbf{k})] = n_\uparrow = 1 - \delta$, and $\mu^* = (\mu - \lambda_\sigma)$ is the effective chemical potential in a paramagnetic state satisfying $(1/N_s) \sum_{\mathbf{k}} \Theta[\mu^* - Z \epsilon(\mathbf{k})] = n_\uparrow = n_\downarrow = (1 - \delta)/2$. The DOS of the FPFM state is the same as the noninteracting DOS $[\rho_0(\epsilon)]$, while the DOS of the PM state is renormalized by a factor Z to $1/Z \times \rho_0(\epsilon/Z)$. Unlike the DMFT method, the slave-boson approach considers only the renormalized quasiparticle DOS ignoring the incoherent contribution. E_{PM} is given by $Z \times E_0$, where E_0 is the noninteracting energy. In other words, as δ reduces to 0, the energy for a paramagnetic state is strongly renormalized by a factor $2\delta/(1+\delta)$ to avoid the doubly occupied states. That makes the FPFM state more stable at small δ .

In Fig. 9(a), FPFM energy and PM energy vs n are shown for $t'/t=0.1, 0$, and -0.1 . For all values of t'/t , the FPFM energy is stable at large n , while the PM energy is stable at small n . The intermediate phase separated region is constructed by the Maxwell construction and is indicative of a first order transition. At large n , as in the plaquette case, the energy curve for the paramagnet state depends weakly on t' while the FPFM energy is reduced with decreasing t'/t . This result is in qualitative agreement with the previous DMFT results. As t'/t decreases, the FPFM state becomes more stable and the critical density n_c decreases. Just as in the DMFT, the large spectral weight of the noninteracting DOS at a low energy makes FPFM state energetically favorable at

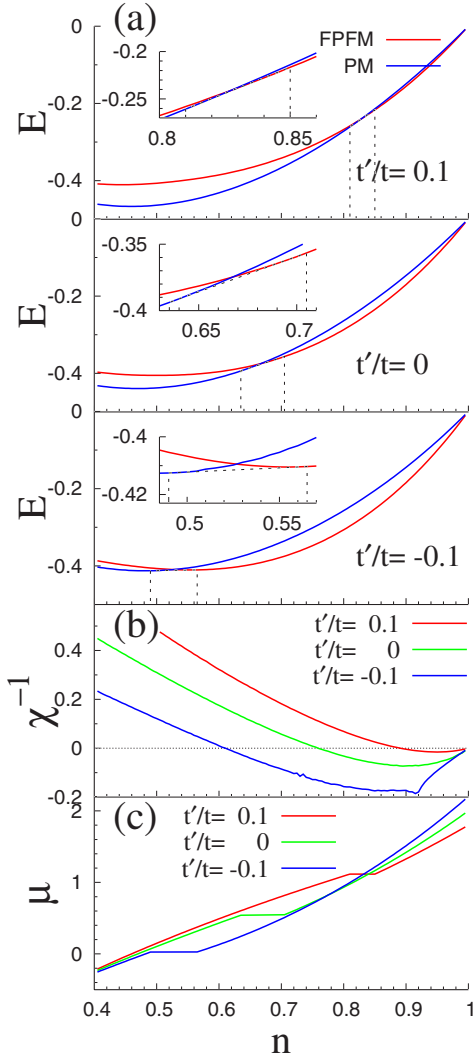


FIG. 9. (Color online) (a) Fully polarized ferromagnetic (FPFM) energy and paramagnetic (PM) energy vs n varying t'/t [0.1 (top), 0 (middle), and -0.1 (bottom)] Inset: maxwell construction to determine the PS region. (b) The inverse of the uniform magnetic susceptibility (χ^{-1}) at $m=0$ vs n varying t'/t (0.1, 0, and -0.1). (c) The chemical potential (μ) vs n at $t'/t=0.1, 0,$ and -0.1 .

$t'/t=-0.1$. When t' is 0, the energy difference between FPFM and PM vanishes at $n_c=2/3$, in agreement with the previous slave-boson calculations.^{8,9}

We also calculate the inverse of uniform magnetic susceptibility (χ^{-1}) to study the instability of the PM state. The analytic expression is

$$\chi^{-1}|_{m=0} = \frac{1}{2\rho(\mu^*)} + \frac{2\mu^*}{1+\delta} + \frac{1}{N_s} \sum_{\mathbf{k}} \frac{4}{(1+\delta)^2} Z\epsilon(\mathbf{k})\Theta[\mu^* - Z\epsilon(\mathbf{k})], \quad (13)$$

where $\rho(\mu^*)$ is the renormalized DOS given by $1/Z \times \rho_0(\mu^*/Z)$.

The trends in χ^{-1} are consistent with the results shown in Fig. 9(a). As t'/t decreases, spin susceptibility diverges at smaller density [see Fig. 9(b)]. However, the divergence of

TABLE I. n_c and the order of the ferromagnetism transition in a $U=\infty$ Hubbard model from both the DMFT+CTQMC approach and the slave-boson approach with $t'/t=-0.1, 0,$ and 0.1 . N/A means no transition to FM state occurs.

		$t'/t=-0.1$	$t'/t=0$	$t'/t=0.1$
DMFT ($T=0.01$)	n_c	0.705	0.815	N/A
	Order	First	Second	N/A
Slave boson ($T=0$)	n_c	0.53	0.67	0.83
	Order	First	First	First

the spin susceptibility does not coincide with the thermodynamic phase transition identified by the total energy differences. The phase transition is thus always first order within the slave-boson approach.

Figure 9(c) shows that a flat chemical potential region exists at any t'/t_s in a μ vs n graph. This is a generic feature of a first-order transition and this region represents the coexistence of the FPFM and PM phases. This coexistence region is larger for negative t'/t favoring transition to the FPFM phase.

V. COMPARISON OF THE SLAVE-BOSON RESULT AND THE DYNAMICAL MEAN-FIELD THEORY PLUS CONTINUOUS TIME QUANTUM MONTE CARLO RESULT

The slave-boson method overestimates the region of the stable FM state as compared to DMFT, and it favors a first-order transition (see Table I). This is because the slave-boson approach overestimates the paramagnetic kinetic energy as compared to the DMFT approach (Fig. 10). The quasiparticle residue Z of the DMFT approach is evaluated by $(1 - \frac{d \text{Im} \Sigma}{d\omega} |_{\omega=0})^{-1}$ on the imaginary frequency axis, while Z of the slave-boson approach is given by $2\delta/(1+\delta)$. Figure 11 shows that Z of the slave-boson study is overestimated as compared to the DMFT+CTQMC case. The slave-boson technique used in this paper is based on the mean-field saddle-point approximation and it does not treat the strong correlation effect properly. Even though DMFT ignores the spatial correlation effect, the temporal correlations are treated exactly by CTQMC. Moreover, the mean-field slave-boson approach evaluates the total energy as the sum of coherent quasiparticle energies [Eq. (12)] while the total energy of DMFT+CTQMC includes contributions from both the incoherent and coherent effects. The overestimated Z in the slave-boson case underestimates the kinetic energy, while the ignorance of contribution from the incoherent part overestimates the energy. As a result, the two errors of the slave-boson approach cancel each other giving a slightly overestimated energy as compared to the DMFT+CTQMC result.

Additionally, the χ^{-1} graph in the slave-boson method almost coincides with the DMFT+CTQMC result comparing Figs. 4 and 9(b). It is not certain how the renormalization residue Z affects χ^{-1} in the DMFT+CTQMC case, and the contribution from the incoherent part is also unclear. Therefore, further study will be required to fully understand the positive agreement of χ in the two methods.

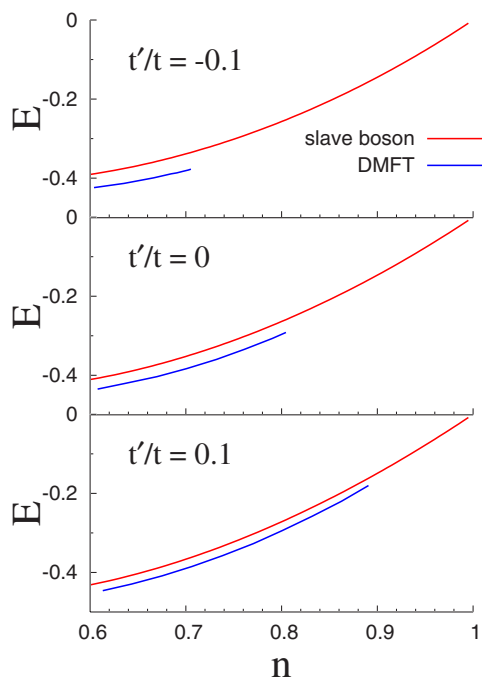


FIG. 10. (Color online) Paramagnetic energy from both the DMFT+CTQMC ($T=0.01$) and the slave-boson ($T=0$) approach vs n at $t'/t=-0.1$ (the top panel), 0 (the middle panel), and 0.1 (the bottom panel).

VI. CONCLUSION

To summarize, we investigated Nagaoka ferromagnetism in the $U=\infty$ Hubbard model including nn hopping t and nnn hopping t' . This model was solved using DMFT with CTQMC and the mean-field slave-boson approach. Even a small value of t'/t yields a significant impact on the stability of Nagaoka ferromagnetism. The DMFT results show that the FM state is more stable for negative t'/t , and this is supported by the slave-boson method (see Table I) and can also be understood from diagonalization of the four-site plaquette. The energy of the minimum spin state ($S=1/2$) depends weakly on t'/t , while the energy of the maximum spin state ($S=3/2$) depends linearly on t'/t . Therefore, the maximum spin state becomes more stable for negative t'/t .

In both slave-boson and DMFT methods, the paramagnetic energy does not vary much with t'/t due to the strong renormalization of the quasiparticle band (see Fig. 10). However, the fully polarized ferromagnetic energy depends on t'/t in a similar fashion as the noninteracting kinetic energy since the correlations are weaker in the broken symmetry state. The negative t'/t gives a high spectral peak in the occupied part of the spectra of the noninteracting system. As a result, the energy of the FM state is lower and the ferromagnetism is stabilized in this case.

Within DMFT, the nature of the transition also varies with t'/t . A first-order transition accompanied by the PS of the FM and PM states occurs at $t'/t=-0.1$, while a second-order transition occurs at $t'/t=0$. In the slave-boson approach, the transition is always first order regardless of t'/t . This is because the slave-boson method overestimates the PM energy. The DMFT result shows that when $n \rightarrow 1$, the FM state be-

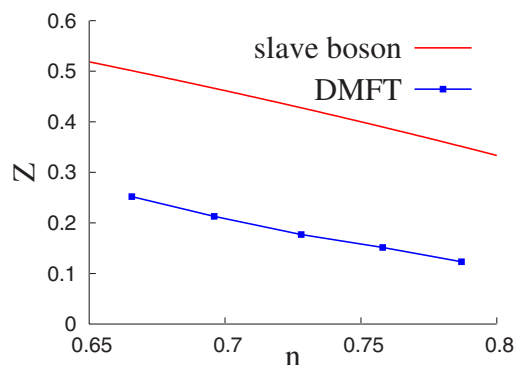


FIG. 11. (Color online) The renormalization residue (Z) of the slave-boson method and the DMFT+CTQMC method ($t'=0$).

comes unstable as T exceeds T_{coh} . In other words, ferromagnetic state is only stable within the coherent Fermi liquid regime.

The $U=\infty$ one-band Hubbard model is a toy model and does not describe any specific material. However, it is physically realizable in an optical lattice due to the recent developments in controlling cold atoms in optical traps.^{28,29} These systems are highly tunable, and the hopping parameter t and the on-site interaction U can be adjusted by varying the ratio of the potential depth of the optical lattice to the recoil energy (V_0/E_R) or the ratio of interatomic scattering length to the lattice spacing (a_s/d). In order to realize the one-band Hubbard model with a large U ($U/t \geq 100$), $V_0/E_R \approx 30$ and $a_s/d \leq 0.01$ should be the range of parameters in the optical lattice (see Fig. 4 of Ref. 29). The tuning of the next-nearest-neighbor hopping t' can be achieved by engineering optical lattices with a nonseparable laser potential over each coordinate axis.

It will be very interesting to test these DMFT results experimentally. Usually, the atomic trap potential is applied to confine atoms in the optical lattice, and the potential varies smoothly having the minimum at the center of the trap. The phase separation between the FM and the PM phases at $t'/t=-0.1$ (taking place between the densities $n=0.696-0.715$) can be observed in the optical lattice as three spatially separated distinct regions. The atom-rich FM region will tend to move to the center of the optical lattice to be energetically stabilized, while the hole-rich PM region will reside on the edge of the optical lattice. Since the total spin is a conserved quantity, the FM region will be located at the center of the trap and will consist of two domains containing the up or down species. Raising the temperature will destroy the ferromagnetic magnetic state and consequently the spatial patterns within the trap.

ACKNOWLEDGMENTS

This research was supported by NSF under Grant No. DMR 0528969. Hyowon Park acknowledges support from the Korea Science and Engineering Foundation Grant funded by the Korea government (MOST) (No. KRF-2005-215-C00050).

- ¹Y. Nagaoka, Phys. Rev. **147**, 392 (1966).
- ²For recent reviews, see P. Fazekas, *Lecture Notes on Electron Correlation and Magnetism*, Series in Modern Condensed Matter Physics Vol. 5 (World Scientific, Singapore, 1999).
- ³B. S. Shastry, H. R. Krishnamurthy, and P. W. Anderson, Phys. Rev. B **41**, 2375 (1990).
- ⁴A. G. Basile and V. Elser, Phys. Rev. B **41**, 4842 (1990).
- ⁵W. von der Linden and D. Edwards, J. Phys.: Condens. Matter **3**, 4917 (1991).
- ⁶T. Hanisch and E. Muller-Hartmann, Ann. Phys. **2**, 381 (1993).
- ⁷P. Wurth, G. Uhrig, and E. Mueller-Hartmann, Ann. Phys. **5**, 148 (1996).
- ⁸B. Moller, K. Doll, and R. Fresard, J. Phys.: Condens. Matter **5**, 4847 (1993).
- ⁹D. Boies, F. Jackson, and A.-M. Tremblay, Int. J. Mod. Phys. B **9**, 1001 (1995).
- ¹⁰X. Y. Zhang, E. Abrahams, and G. Kotliar, Phys. Rev. Lett. **66**, 1236 (1991).
- ¹¹F. Becca and S. Sorella, Phys. Rev. Lett. **86**, 3396 (2001).
- ¹²A. M. Oles and P. Prelovsek, Phys. Rev. B **43**, 13348 (1991).
- ¹³H. Tasaki, Phys. Rev. Lett. **69**, 1608 (1992).
- ¹⁴E. Gagliano, S. Bacci, and E. Dagotto, Phys. Rev. B **42**, 6222 (1990).
- ¹⁵T. Hanisch, G. S. Uhrig, and E. Muller-Hartmann, Phys. Rev. B **56**, 13960 (1997).
- ¹⁶J. Wahle, N. Blumer, J. Schlipf, K. Held, and D. Vollhardt, Phys. Rev. B **58**, 12749 (1998).
- ¹⁷L. Arrachea, Phys. Rev. B **62**, 10033 (2000).
- ¹⁸M. Ulmke, Eur. Phys. J. B **1**, 301 (1998).
- ¹⁹T. Wegner, M. Potthoff, and W. Nolting, Phys. Rev. B **57**, 6211 (1998).
- ²⁰R. Hlubina, S. Sorella, and F. Guinea, Phys. Rev. Lett. **78**, 1343 (1997).
- ²¹T. Obermeier, T. Pruschke, and J. Keller, Phys. Rev. B **56**, R8479 (1997).
- ²²R. Zitzler, T. Pruschke, and R. Bulla, Eur. Phys. J. B **27**, 473 (2002).
- ²³P. Werner, A. Comanac, L. de' Medici, M. Troyer, and A. J. Millis, Phys. Rev. Lett. **97**, 076405 (2006).
- ²⁴K. Haule, Phys. Rev. B **75**, 155113 (2007).
- ²⁵M. Jarrell and J. Gubernatis, Phys. Rep. **269**, 133 (1996).
- ²⁶H. Kajueter, G. Kotliar, and G. Moeller, Phys. Rev. B **53**, 16214 (1996).
- ²⁷A. M. Polyakov, Phys. Lett. **59B**, 79 (1975).
- ²⁸D. Jaksch and P. Zoller, Ann. Phys. **315**, 52 (2005).
- ²⁹A. Georges, Lectures given at the Enrico Fermi Summer School on Ultracold Fermi Gases, Varenna, Italy, June 2006 (unpublished).